Supplemental Materials

Description of the simple STDP model

The detailed molecular STDP model is based on ion channel activities and signal transduction (Urakubo et al., 2008; Urakubo et al., 2009). We simplified the detailed molecular STDP model and made a simple STDP model (Honda et al., 2009), comprised of 8 ordinary differential equations based on a kinetic reaction. The following is a schematic diagram of the simple STDP model. The arrows and lines with a black circle indicate the stimulatory and inhibitory interactions, respectively. The molecules required for LTP and LTD are enclosed by red and blue squares, respectively.

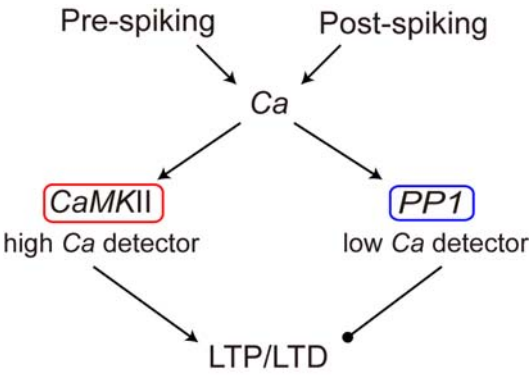

The computational cost of the simple STDP model is much lower than that of the detailed molecular STDP model. In the simple STDP model, the timings of the pre- and post-spiking are translated into changes in synaptic strengths. A detailed description follows.

Pre- and post-spiking induce Ca^{2+} entry into a post-neuron. We modelled these process using a presynaptic short-term depression (Matveev and Wang, 2000). The equations are as follows:

$$\frac{dNMDAR(t)}{dt} = -\frac{NMDAR(t)}{\tau_{NMDAR}}, \tag{1}$$

$$\frac{dV(t)}{dt} = -\frac{V(t)-V_{rest}}{\tau_V}, \tag{2}$$

$$\frac{dCa(t)}{dt} = NMDAR(t)\cdot\left(0.0223\cdot\left(V(t)-V_{rest}\right)+0.5\right)-\frac{Ca(t)}{\tau_{Ca}}, \tag{3}$$

$$\begin{aligned} &\text{if } \ t=t_{post} \quad \text{then } \ V(t)\leftarrow V(t)+AP, \quad Ca(t)\leftarrow Ca(t)+Ca_{VGCC}\ , \\ &\text{if } \ t=t_{pre} \quad \text{then } \ NMDAR(t)\leftarrow NMDAR(t)+\frac{K_{\mathrm{Ca}}}{K_{\mathrm{Ca}}+Ca(t)}, \end{aligned} \tag{4}$$

where *NMDAR* (*t*), *V*(*t*) and *Ca*(*t*) represent the NMDAR activity, membrane potential, and Ca^{2+}·CaM concentration, respectively; τ_{NMDAR} τ_V and τ_{Ca} are the decay time constants of *NMDARs*(*t*), *V*(*t*) and *Ca*(*t*), respectively; V_{rest} is the resting membrane potential; *AP* is the amplitude of the backpropagating action potential; Ca_{VGCC} is the Ca^{2+} influx via VGCC; K_{Ca} is the effective *Ca* that produces a 50% inhibition of the maximal activity of *NMDAR*; t_{pre} and t_{post} are the timings of the pre-spiking and post-spiking, respectively.

Equations 1 and 2 represent the decays of the NMDAR activity and membrane potential, respectively. Equation 3 represents that Ca^{2+} increase that depends on the voltage-dependent activation of the NMDARs with an exponential decay, where $[0.0223(V(t) - V_{rest}) + 0.5]$ denotes the voltage-dependence of the NMDARs. In Equation 4, at $t = t_{post}$, post-spiking triggers the increase in the voltage via bpAP and a Ca^{2+} increase via VGCC, whereas, at $t = t_{pre}$, *NMDAR* is activated in a reciprocal manner to that of *Ca*. Equations 3 and 4 indicate that *Ca* acts on *NMDAR* only at $t = t_{pre}$

but not later, which means that the suppression of NMDARs reflects the Ca^{2+} level at pre-spiking, but not after pre-spiking. Thus, Equations 3 and 4 represent the allosteric kinetics of NMDARs.

The model for short-term depression (Matveev and Wang, 2000) is a simple model of synaptic vesicle turnover. The description of the model is as follows:

$$\begin{aligned} P(t) &= 1-\exp\left[-\alpha N(t)\right] \\ N(t) &= \max\left[0,\, N_0 - \sum_{t>t_j^{syn}} v(t-t_j^{syn})\right], \\ v(t') &= \exp(-t'/\tau_D)\cdot H(t') \end{aligned} \qquad (5)$$

where $P(t)$ is the probability of glutamate release at a synapse; $N(t)$ and $v(t)$ are the number of vesicles available and unavailable for release, respectively; N_0 is the maximum vesicle number; α is the fusion rate constant; τ_D is the recovery time constant; t_j^{syn} is the time of the j^{th} glutamate release event; and $H(t)$ is the Heaviside step function. When a pre-spiking occurs at t_i^{pre}, a glutamate release event occurs with the probability $P(t_i^{pre})$, and the event is counted as the j^{th} glutamate release ($t_j^{syn} \leftarrow t_i^{pre}$). The parameter values and the initial values are listed in Table A.

Ca^{2+} activates Ca^{2+}-dependent signal transduction cascades and induces a change in synaptic strengths. We modified the CaMKII model (Dupont et al., 2003) by incorporating the activation of CaMKII by CaMKII-binding scaffold proteins (Scaffold) such as NMDARs, and described this process as follows:

$$\frac{dPP1(t)}{dt} = k_1\left(1-PP1(t)\right)Ca(t)^3 - k_2 PP1(t)\cdot Ca(t)^5 - k_3\left(PP1(t)-PP1_{basal}\right), \qquad (6)$$

$$\frac{dCaMK\text{II}\,b(t)}{dt} = \left(k_4 Ca(t)^4 + \varepsilon\right)\left(1 - T_{act}(t)\right) - k_5 \cdot CaMK\text{II}\,b(t) - V_f + V_b$$
$$\frac{dCaMK\text{II}\,p(t)}{dt} = V_f - V_b$$
$$V_f = k_6\left(-0.220T_{act}(t) + 1.826T_{act}(t)^2 - 0.800T_{act}(t)^3\right)T_{act}(t) \cdot CaMK\text{II}\,b(t) \quad , \qquad (7)$$
$$V_b = k_7 \cdot CaMK\text{II}\,p(t)$$

$$\frac{dSS(t)}{dt} = k_8\left(SS_{\max} - SS(t)\right)T_{act}(t) - k_9 SS(t)PP1(t), \qquad (8)$$

where $PP1(t)$, $CaMK\text{II}b(t)$, $CaMK\text{II}p(t)$, and $SS(t)$ represent the PP1 activity, Ca^{2+}-bound CaMKII activity, phosphorylated CaMKII activity and normalised synaptic strength, respectively; $PP1_{basal}$ and SS_{max} indicate the basal PP1 activity and normalised maximal synaptic strength, respectively; k_1 and k_3 are the effective forward and backward rate constants of PP1 activation, respectively; k_2 is the effective time constant of PP1 inhibition; k_4 and ε are the effective forward binding constants of Ca^{2+} and Scaffold, to CaMKII, respectively; k_5 is the dissociation rate of Ca^{2+} and NMDAR from CaMKII; k_6 and k_7 are the effective phosphorylation and dephosphorylation time constants of CaMKII, respectively; and k_8 and k_9 are the effective forward and backward rate constants of synaptic strength, respectively. Because both Ca^{2+}-bound and phosphorylated CaMKII are active forms, we defined the active forms of CaMII, or $T_{act}(t)$, as $T_{act}(t) = CaMK\text{II}b(t) + CaMK\text{II}p(t)$. V_f and V_b are the phosphorylation and dephosphorylation rate of CaMKII, respectively. The former function is the empirical cubic function of the autophosphorylation of CaMKII.

Equation 6 represents the activity of PP1, which is activated and inhibited at low and high levels of Ca^{2+}, respectively. Equation 7 represents the activity of CaMKII. Ca^{2+} binds to CaMKII and induces the successive autophosphorylation of CaMKII subunits, leading to the persistent activation of CaMKII. Equation 8 represents the normalized synaptic strength, which is enhanced and suppressed by activated

CaMKII and PP1, respectively. See Table B for the parameter values and the initial values.

This simple STDP model can reproduce various experimentally observed synaptic modificationsl, such as spike doublet-, triplet-, quadruplet-, and burst-dependent synaptic plasticity (Froemke and Dan, 2002; Froemke et al., 2006; Urakubo et al., 2008; Honda et al., 2009). The detailed features of this simple STDP model will be analyzed in another project.

Table A. Parameters and initial values

parameters			parameters		initial values	
τ_{NMDAR}	30	ms	AP	50	$NMDAR(0)$	0
τ_V	6	ms	Ca_{VGCC}	0.8	$V(0)$	0
τ_{Ca}	18	ms	K_{Ca}	0.35	$Ca(0)$	0
τ_D	300	ms	α	3		
V_{rest}	-65		N_0	1.5		

Table B. Parameters and initial values

parameters			parameters			initial values	
k_1	0.16	s^{-1}	k_7	0.01	s^{-1}	$PP1(0)$	0.1
k_2	0.078	s^{-1}	k_8	0.18	s^{-1}	$CaMKIIb(0)$	0.157
k_3	0.144	s^{-1}	k_9	0.295	s^{-1}	$CaMKIIp(0)$	0.007
k_4	0.002	s^{-1}	ε	0.03	s^{-1}	$SS(0)$	1
k_5	0.16	s^{-1}	$PP1_{basal}$	0.1			
k_6	0.29	s^{-1}	SS_{max}	2			

Supplemental figures and figure legends

Supplemental Figure 1

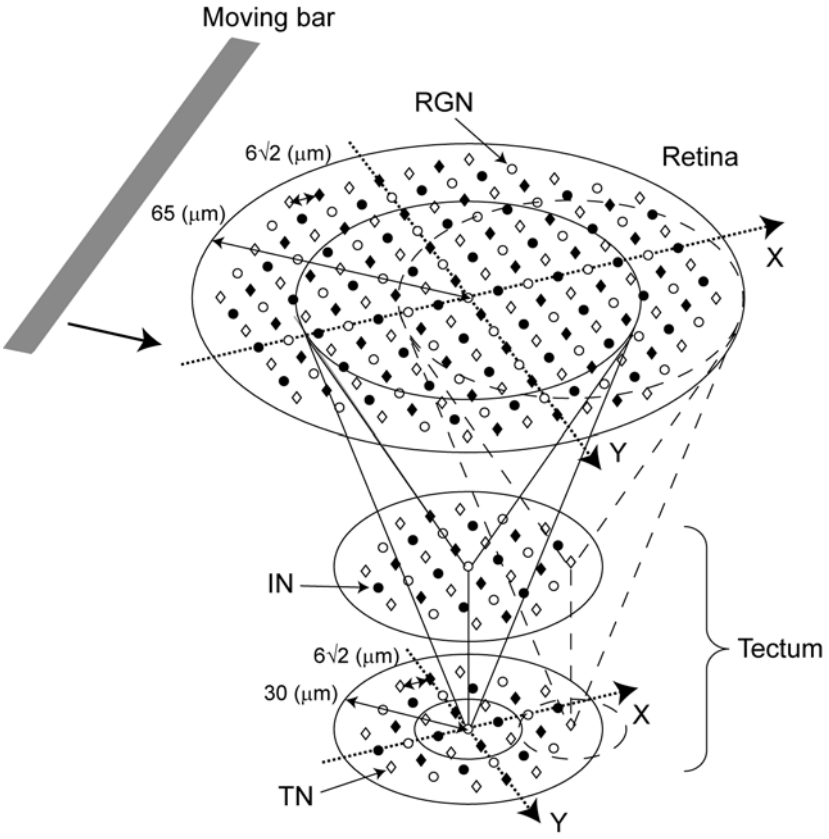

Supplemental Figure 2

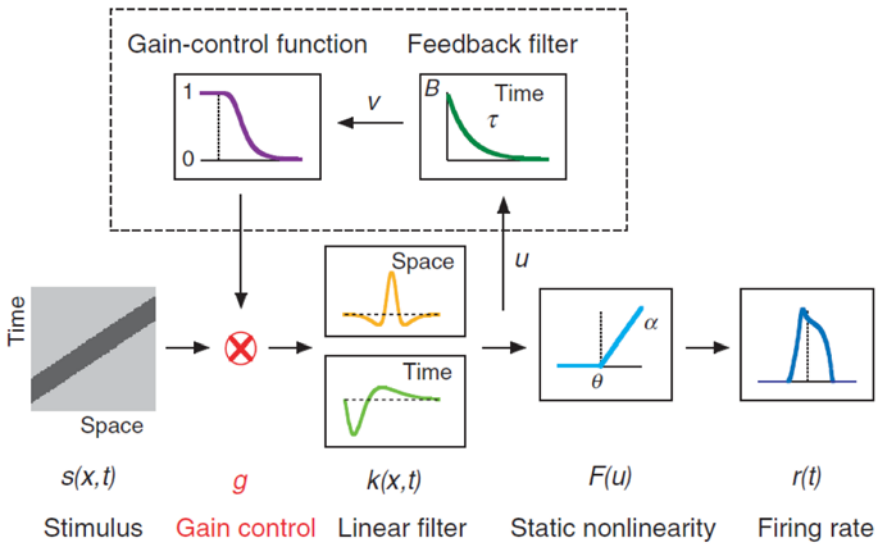

Supplemental Figure 3

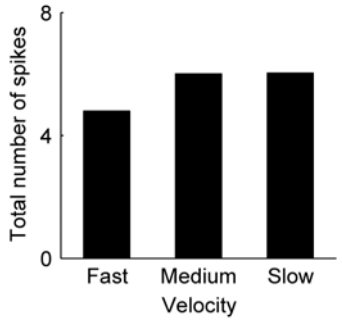

Supplemental Figure 4

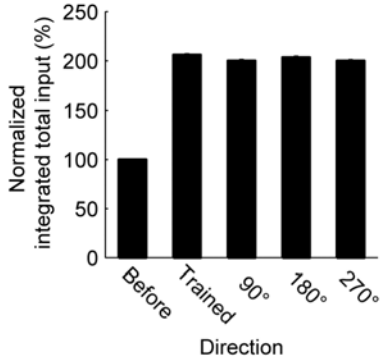

Supplemental Figure 5

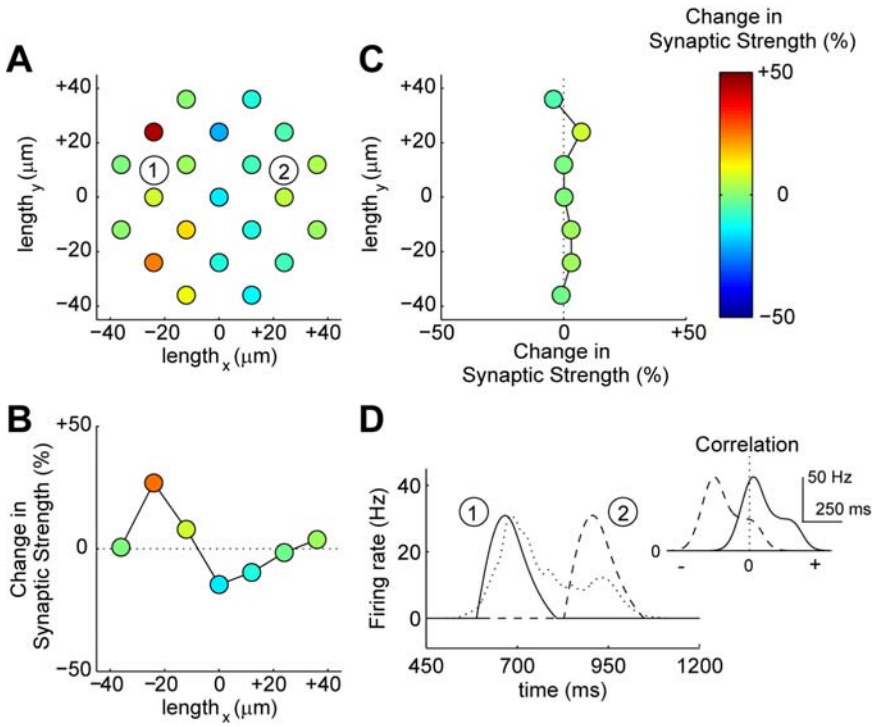

Supplemental Figure 6

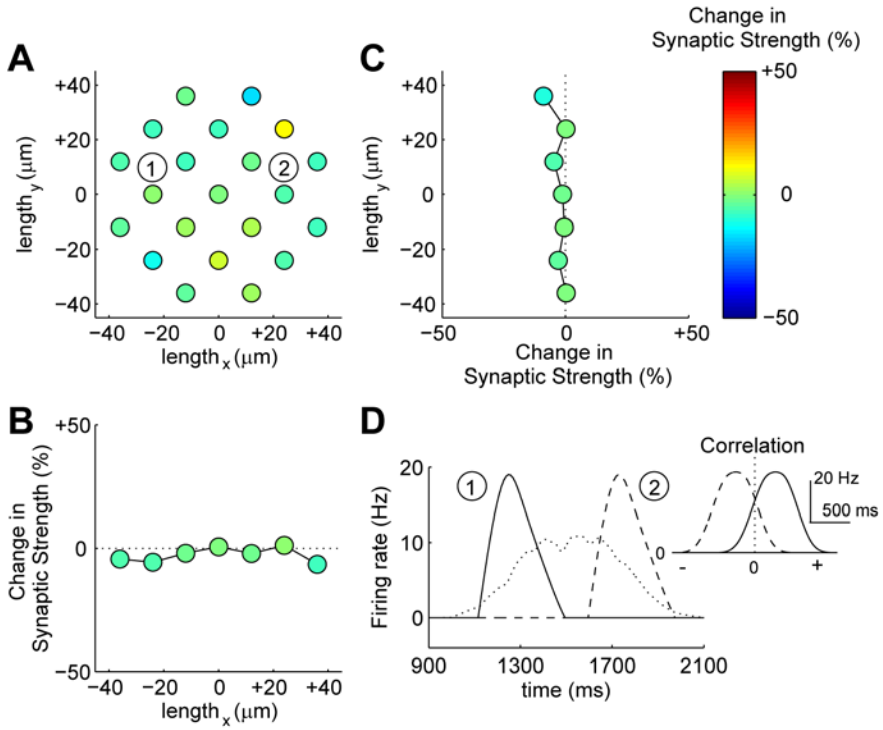

Supplemental Figure 7

A, Normalized inhibitory amplitude = 0

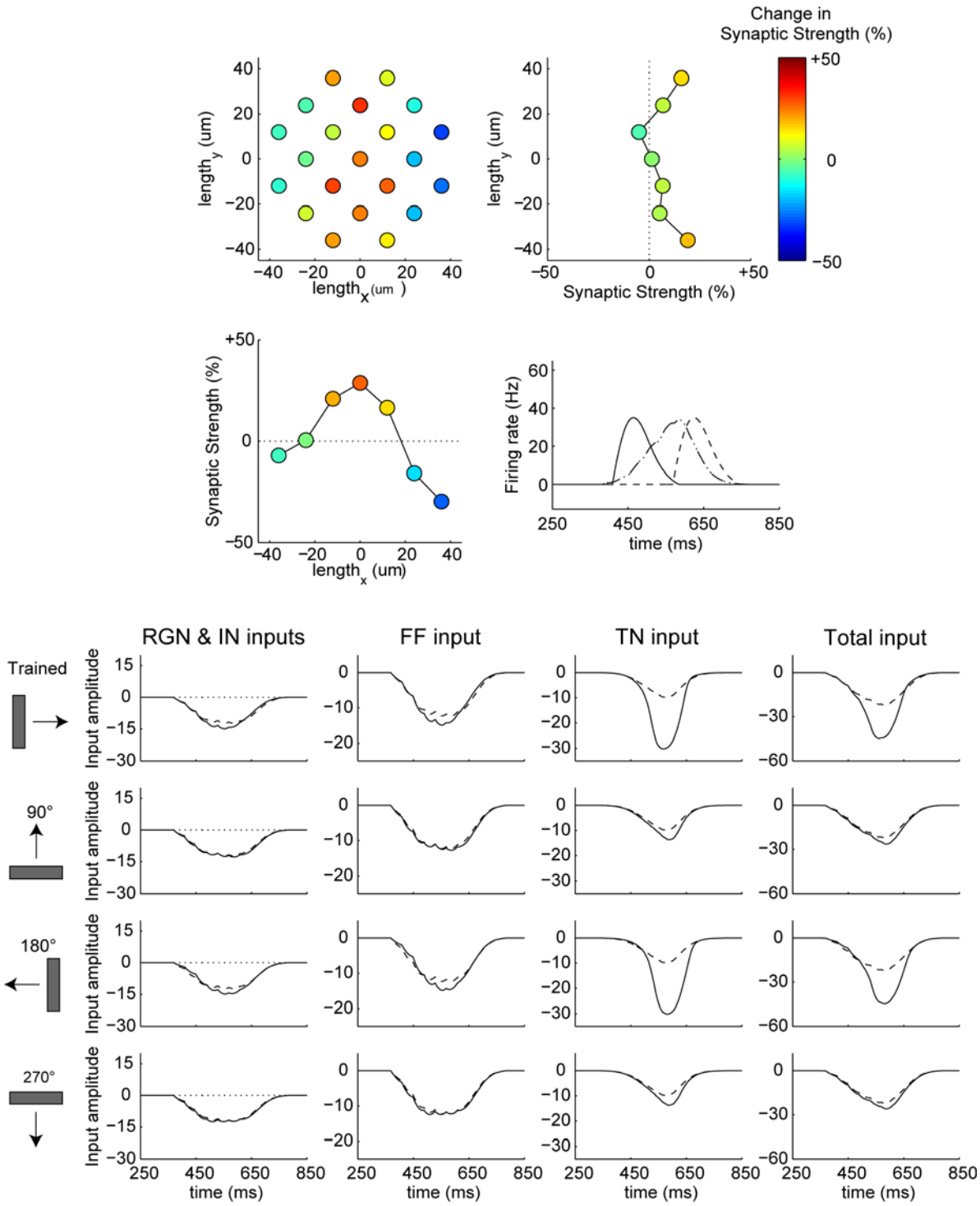

B, Normalized inhibitory amplitude = 0.5

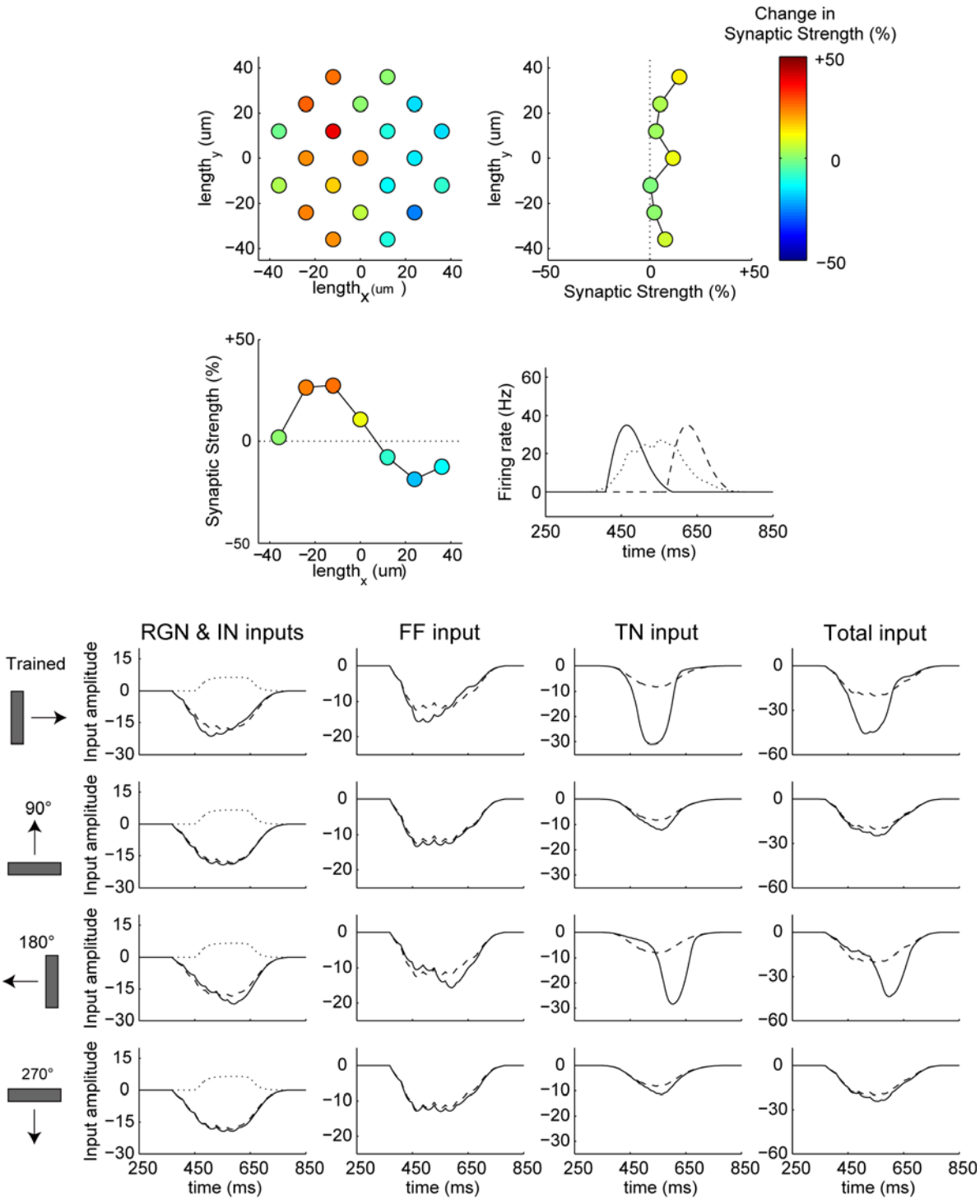

C, Normalized inhibitory amplitude = 1.0

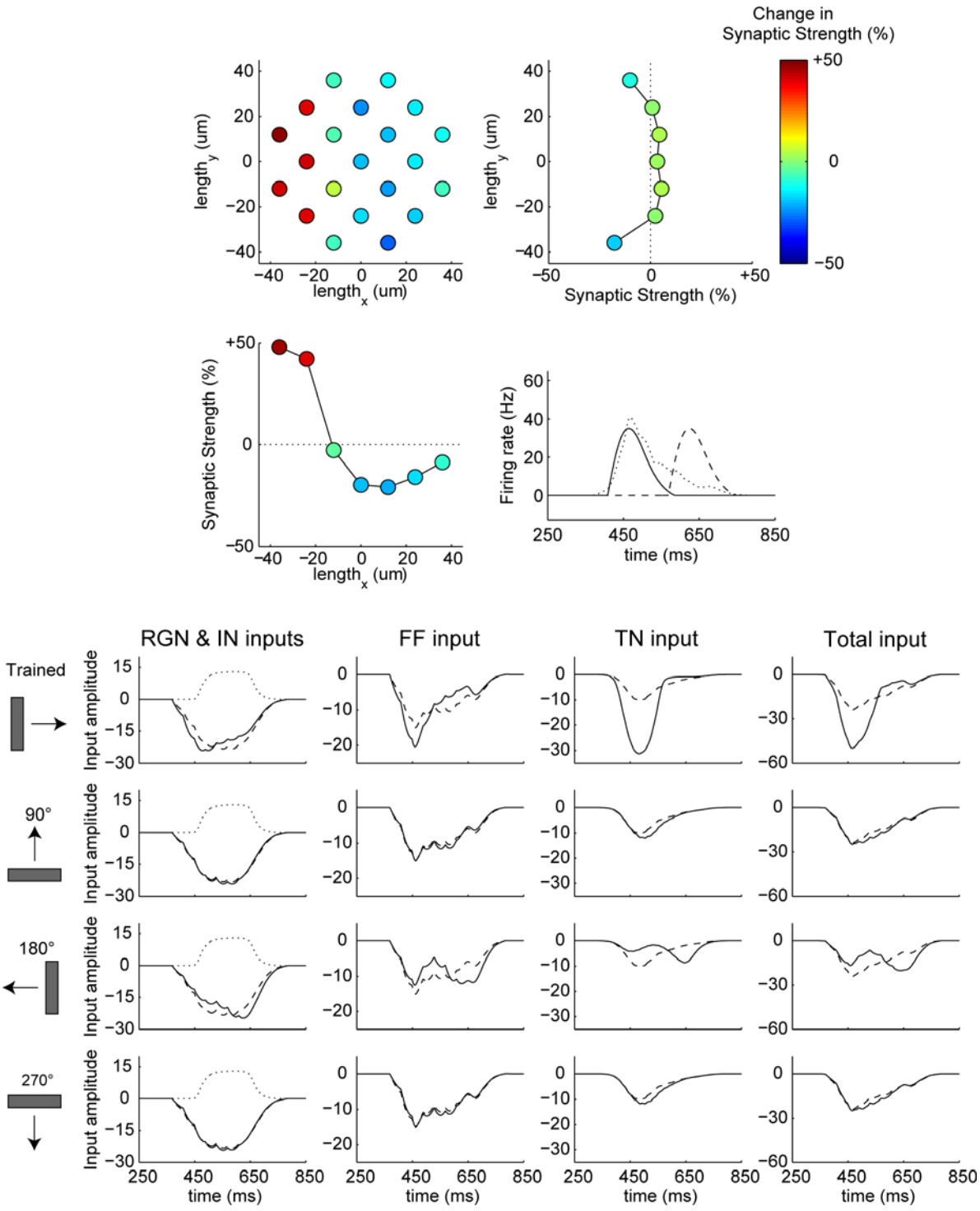

D, Normalized inhibitory amplitude = 1.5

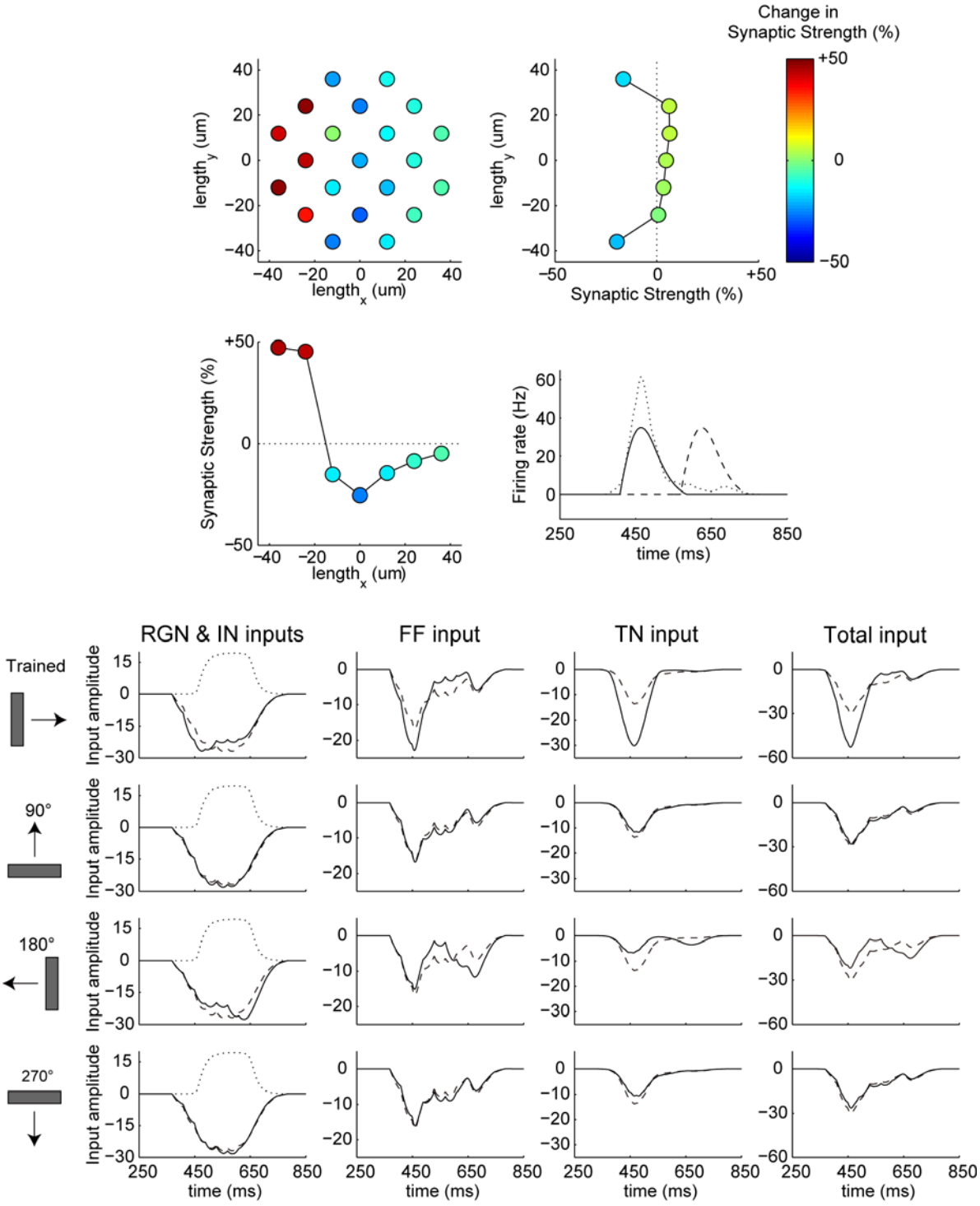

Supplemental Figure 1. Structure of the retinotectal circuit model. The retinotectal circuit model consists of one retinal and two tectal layers. The retinal layer was two-dimensional lattice in a circle with radius 65 μm, and one RGN was located at each lattice point (185 RGNs in total). The distance between nearest lattice points, or the distance between nearest RGNs was $6\sqrt{2}$ μm. The first tectal layer was two-dimensional lattice in a circle with radius 30 μm, and one IN was located at each lattice point (37 INs in total). The distance between nearest INs was $6\sqrt{2}$ μm. The second tectal layer was two-dimensional lattice in a circle with radius 30 μm, and one TN was located at each lattice point (37 TNs in total). The distance between nearest TNs was $6\sqrt{2}$ μm. The lattice orientations were the same across all three layers. All neurons are indicated by four different symbols (open circles, filled circles, open diamonds, and filled diamonds). The coordinate of the neuron was represented as (x, y) (μm). The position of the neuron located at the center in each layer was represented as (0, 0). The IN located at the position (x, y) on the first tectal layer received excitatory input from 21 RGNs indicated by the same symbol, which were located within a circle with center (x, y) and radius 40 μm on the retinal layer, and sent inhibitory input to the TN located at the position (x, y) on the second tectal layer. The same 21 RGNs also sent excitatory input to the TN located at the position (x, y). The TN located at the position (x, y) received excitatory input from the neighboring TNs located within a circle with center (x, y) and radius 12.5 μm. The solid and dashed lines indicate the cases (x, y) = (0, 0) and (x, y) = $(18\sqrt{2}, 6\sqrt{2})$ (μm), respectively. The directions of moving bars are chosen from 45°, 135°, 215°, or 305° from the X-axis.

Supplemental Figure 2. LN cascade model for the light response of an RGN (adopted from Berry et al., 1999). The visual stimuli is multiplied by a gain factor, convolved with the spatial and temporal linear filters, and rectified by the static nonlinear function to produce the firing rate. The contrast-gain control mechanism (boxed region) takes the output of the linear filters, and sets the gain factor.

Supplemental Figure 3. The total number of spikes of the centered TN is constant regardless of the speeds of the moving bars. The total numbers of spikes of the centered TN evoked by the sweep of fast, medium-speed and slow moving bars before training (one trial) are shown.

Supplemental Figure 4. Suppression of feedforward inhibition leads to a loss of direction selectivity. The percentage changes in the integrated total input in each direction before and after the suppression of feedforward inhibition (averages of five trials ± SEM) are shown. After training, the synaptic strengths between the INs and the TNs were adjusted to zero, and the simulations were performed.

Supplemental Figure 5. Asymmetric synaptic modification through STDP using a medium-speed moving bar as a training stimulus. ***A***-***C***, Change in the synaptic strengths (one trial). ***A***, Changes in the synaptic strengths from each RGN to the TN. The coordinates show the relative position of each RGN to the TN. The circles indicate the locations of each RGN, and the colors represent the amplitude of the change in the

synaptic strengths. The trained direction is left-to-right. ***B***, ***C***, Averaged changes in the synaptic strengths in the horizontal (***B***) and perpendicular (***C***) orientations against the trained direction. ***D***, Time profiles of the firing rates of two RGNs (solid and dashed lines) indicated in (***A***) and the TN (dotted line). The numbers of the RGNs correspond to those in (***A***). The inset shows cross-correlations of the firing rates between each RGN and the TN. The colors correspond to those shown in (***D***).

Supplemental Figure 6. Synaptic strengths were not modified using a slow moving bar as a training stimulus. ***A***-***C***, Change in the synaptic strengths (one trial). ***A***, Changes in the synaptic strengths from each RGN to the TN. The coordinates show the relative position of each RGN to the TN. The circles indicate the locations of each RGN, and the colors represent the amplitude of the change in the synaptic strengths. The trained direction is left-to-right. ***B***, ***C***, Averaged changes in the synaptic strengths in the horizontal (***B***) and perpendicular (***C***) orientations against the trained direction. ***D***, Time profiles of the firing rates of two RGNs (solid and dashed lines) indicated in (***A***) and the TN (dotted line). The numbers of the RGNs correspond to those in (***A***). The inset shows cross-correlations of the firing rates between each RGN and the TN. The colors correspond to those shown in (***D***).

Supplemental Figure 7. Developmental process at different inhibitory amplitudes. ***A***-***D***, Changes in the synaptic strengths and time profiles of each input through training in the

case of normalized inhibitory amplitude = 0 (***A***), 0.5 (***B***), 1 (***C***), or 1.5 (***D***) (one trial each). The upper panels represent the changes in the synaptic strengths from each RGN to the TN. The lower panels represent the time profiles of the RGN input, IN input (dotted lines), FF input, TN input, and total input evoked by fast bars moving in the four orthogonal directions before (dashed lines) and after (solid lines) training.

References

Berry MJ, 2nd, Brivanlou IH, Jordan TA, Meister M (1999) Anticipation of moving stimuli by the retina. Nature 398:334-338.

Dupont G, Houart G, De Koninck P (2003) Sensitivity of CaM kinase II to the frequency of Ca2+ oscillations: a simple model. Cell Calcium 34:485-497.

Froemke RC, Dan Y (2002) Spike-timing-dependent synaptic modification induced by natural spike trains. Nature 416:433-438.

Froemke RC, Tsay IA, Raad M, Long JD, Dan Y (2006) Contribution of individual spikes in burst-induced long-term synaptic modification. J Neurophysiol 95:1620-1629.

Honda M, Urakubo H, Kuroda S (2009) Acquirement of direction selectivity through STDP in retinotectum. Neuroscience Research 65:S65-S65.

Matveev V, Wang XJ (2000) Implications of all-or-none synaptic transmission and short-term depression beyond vesicle depletion: a computational study. J Neurosci 20:1575-1588.

Urakubo H, Honda M, Froemke RC, Kuroda S (2008) Requirement of an allosteric kinetics of NMDA receptors for spike timing-dependent plasticity. J Neurosci 28:3310-3323.

Urakubo H, Honda M, Tanaka K, Kuroda S (2009) Experimental and computational aspects of signaling mechanisms of spike-timing-dependent plasticity. Hfsp J 3:240-254.